Hindawi
Advances in Polymer Technology
Volume 2024, Article ID 3623198, 10 pages
https://doi.org/10.1155/2024/3623198

Research Article

Effects of SiO_2 Nanoparticles on Polyvinyl Alcohol/Carboxymethyl Cellulose Polymer Blend Films' Structural, Wettability, Surface Roughness, and Optical Characteristics

T. S. Soliman [1,2]

[1]*Physics Department, Faculty of Science, Benha University, Benha 13518, Egypt*
[2]*Institute of Natural Sciences and Mathematics, Ural Federal University, Ekaterinburg 620000, Russia*

Correspondence should be addressed to T. S. Soliman; tarek.attia@fsc.bu.edu.eg

Received 20 March 2024; Revised 22 April 2024; Accepted 27 April 2024; Published 7 May 2024

Academic Editor: Chenggao Li

The blend matrix composed of polyvinyl alcohol and carboxymethylcellulose (PVA/CMC) was prepared via the casting method. SiO_2 nanoparticles were added as reinforcement in different amounts ($SiO_2 = 1$, 2, 3, and 4 wt.%). The study utilized FTIR to examine the alterations in composition and the interplay between the blend matrix and the inclusion of SiO_2. Also, for the first time, the surface roughness and surface wettability of the PVA/CMC blend matrix were investigated with the addition of SiO_2 using measurements of contact angle and surface roughness parameters. The surface roughness and wettability of the blend matrix increased as the SiO_2 content increased. In addition, the blend matrix optical features were determined by the UV–visible spectrophotometer. Based on the analysis using Tauc's relation, it was found that the energy bandgap decreases from 5.52 to 5.17 eV (direct transition) and from 4.79 to 4.32 eV (indirect transition) for the PVA/CMC and PVA/CMC/4%SiO_2 blend films, respectively. The refractive index increases from 2.009 to about 2.144 for the PVA/CMC and PVA/CMC/4%SiO_2 blend films, respectively. Furthermore, optical conductivity and dielectric constants were improved for the PVA/CMC blend film after the addition of SiO_2 nanoparticles.

1. Introduction

Blended polymers are a hot topic in the scientific community due to their remarkable physicochemical properties [1, 2]. The optical properties of blended polymers make them a compelling and promising area of research. Researchers have been eagerly exploring their possible uses in various fields, like electronics, energy, and medicine [3]. These mixed films have consistently proven to be superior in terms of performance, durability, and versatility. Mixed films are the clear choice for developing cutting-edge electronics or simply seeking to improve existing technology [1, 4–7]. Blended polymers have the unique ability to modify their structure and composition to customize their optical behavior, which makes them very promising for creating innovative technologies.

Polyvinyl alcohol and sodium carboxymethylcellulose (PVA and CMC) are compatible polymers that form highly transparent blend films. PVA and CMC share characteristics like water solubility, nontoxic, abundant, cross-linked, and biodegradable polymers [8]. CMC is a pH-sensitive ionic polyelectrolyte with carboxyl groups [9]. The combination of CMC and PVA presents an opportunity to achieve the benefits of both materials. In addition, the presence of the hydroxyl (OH) groups in the backbone of PVA and CMC may lead to the formation of inter- and intra-hydrogen bonds [5, 10].

Metal oxide–polymer composites have recently gained significant research interest for their applications in catalysis, electronics, photonics, and optoelectronics [11]. Additives of nanosized inorganic particles in the polymeric matrix create nanocomposites with unique properties distinct from conventional materials [11–17]. Recently, ferrite nanoparticles

were used as additives in a PVA/CMC blend matrix to tune the optical parameters to be used in various optical applications [18, 19]. SnS [20–22], $Co_{0.9}Cu_{0.1}S$ [23], and Ag/CuS [24] nanoparticles were added to the PVA/polyvinyl propylene (PVP) blend film to adjust its optical parameters and make it suitable for optoelectronic applications. PVA/PVP blend films reinforced with SiO_2 have previously been discussed in terms of their structural and optical properties [25, 26]. The use of SiO_2 as a nanofiller for PVA/CMC blend films was rarely discussed. The influence of SnO_2/SiO_2 and Cr_2O_3/SiO_2 nanocomposites on the optical parameters and structural features of the PVA/CMC matrix have been discussed [27, 28]. The integration of SiO_2 nanoparticles has played a pivotal role in revolutionizing the enhancement of polymer surfaces' morphological structure and optical characteristics. Previously, the PVA matrix doped with various content of SiO_2 nanoparticles showed an increase in the hydrophilicity, as the water contact angle with the film surface was found to decrease with increasing the SiO_2 content in the PVA matrix [29]. While, SiO_2 nanoparticles were observed to enhance the hydrophobicity and raise the roughness of the PVDF-HFP films [30]. Also, the optical properties and wettability of the polystyrene films were affected by the inclusion of SiO_2 in the matrix [31]. SiO_2 was found to play a vital role in changing the wettability of polymer films [29, 31].

Herein, novel PVA/CMC films reinforced with different amounts of SiO_2 are fabricated. In addition, the wettability and surface roughness properties of the blend matrix are investigated for the first time, as is the influence of various concentrations of silica on it. To characterize the functional groups of the prepared films, Fourier transform infrared spectroscopy was used. Moreover, the surface roughness and the water contact angle were investigated. Utilizing the absorption and transmission data from UV–visible spectroscopy, one can accurately estimate the optical parameters of PVA/CMC/SiO_2 films. This approach provides a reliable and efficient way to analyze these films, providing valuable insights to both academics and business experts.

2. Experimental and Characterization

PVA/CMC films were prepared by casting the solution. First, PVA (molecular weight (M_η) = 1×10^6, QualiChem's company, India) and CMC (0.7° of substitution and $M_\eta = 1 \times 10^5$) powders, with a ratio of 80/20, were dissolved separately in distilled water. Subsequently, the polymer solutions were blended by adding the PVA solution to the CMC solution while stirring constantly at room temperature for 2 hr, until a homogenous mixture was achieved. Then, the prepared PVA/CMC blend solution was divided into five flaxes; one of them was pristine without additive, and the others were reinforced with $x SiO_2$ ($x = 0$, 1, 2, 3, and 4 wt.%) using probe ultrasound procedure. After the distribution of SiO_2 nanoparticles in the blend matrix, the mix was poured into Petri plates and left to dry at room temperature (25°C) for several days. The prepared samples with 0, 1, 2, 3, and 4 wt.% SiO_2 in PVA/CMC blend were lapeled as PCS0, PCS1, PCS2, PCS3, and PCS4, respectively. Finally, the prepared films with approximately a thickness of about 100 μm were utilized for measurements. The position and intensity of the chemical bonds of the films before and after the inclusion of various SiO_2 concentrations were recorded via Fourier transform infrared (FTIR) spectroscopy. A roughness tester (SRT-6600) was utilized to measure the surface roughness of the polymer films. This tester relies on a moving sensor on the film surface to identify a roughness profile curve and instantly record the roughness parameters. The wettability of the PVA/CMC blend films can be accurately determined by measuring the contact angles using the reliable Ossila Digital Goniometer (Model L2004A1, Sheffield, UK), with an accuracy ±1°. An ultraviolet–visible spectrometer was used to measure the blend films' absorbance both before and after SiO_2 was added.

3. Results and Discussion

3.1. FTIR, Contact Angle, and Surface Roughness Analysis. Figure 1 shows PCS films' FTIR spectra. The bond positions and assignments for the pristine PVA/CMC are presented in Table 1.

The broadband in the region 3,200–3,500 cm^{-1} is assigned to —OH group. The fingerprint bands in the region from 1,500 to 400 cm^{-1} show the characteristics bond of PVA and CMC. The band observed at 1,070 cm^{-1} is related to C—O bond of CMC, and the same band also was assigned for PVA. The SiO_2 impact on the vibrational modes in terms of a reduction or increase in band intensity with increasing SiO_2 content was observed due to crosslinking with the blend functional groups. For the pristine sample (PCS0), the bond at 2,166 cm^{-1} was shifted to higher wavenumber at 2,167, 2,168, 2,169, and 2,169 cm^{-1} for PCS1, PCS2, PCS3, and PCS4, respectively. The bands at 957 and 856 cm^{-1} are assigned to the stretching of CH_2 and C—C bonds, respectively. These bands are slightly shifted with increasing SiO_2 concentration in the PVA/CMC film, as shown in Figure 1(b). The band at 920 cm^{-1} is linked to the C—C stretching band of PVA was vanished with the inclusion of higher content of SiO_2 nanoparticles, which might be due to the destruction of this bond and formation of the new bond Si—O—C [37, 40]. The band at 1,095 cm^{-1}, which is related to both PVA and CMC [41], ascribed to the C—O bond of the PCS0 sample, was shifted to 1,079 cm^{-1} after the inclusion of 4 wt.% SiO_2. This is ascribed to the combination of the Si—O band of the silica at 1,060 cm^{-1} with the C—O bond of the polymer blend matrix [40]. Besides the weak band observed at 1,234 cm^{-1} which attributed to the Si—O—Si asymmetric vibrations [36, 42]. In addition, the Si—O—Si stretching mode at 800 cm^{-1} at the higher content of SiO_2 nanoparticles testified to the presence of SiO_2 in the blend matrix, as mentioned elsewhere [36, 40]. The FTIR analysis results are conclusive; they show that the PVA/CMC blend and SiO_2 have a clear and specific interaction. These findings demonstrate the potential for this blend to offer unique benefits and applications in the field.

The interaction between the liquid and solid surfaces is highly dependent on surface-free energy, and it is the main parameter that influences the wetting property. The contact

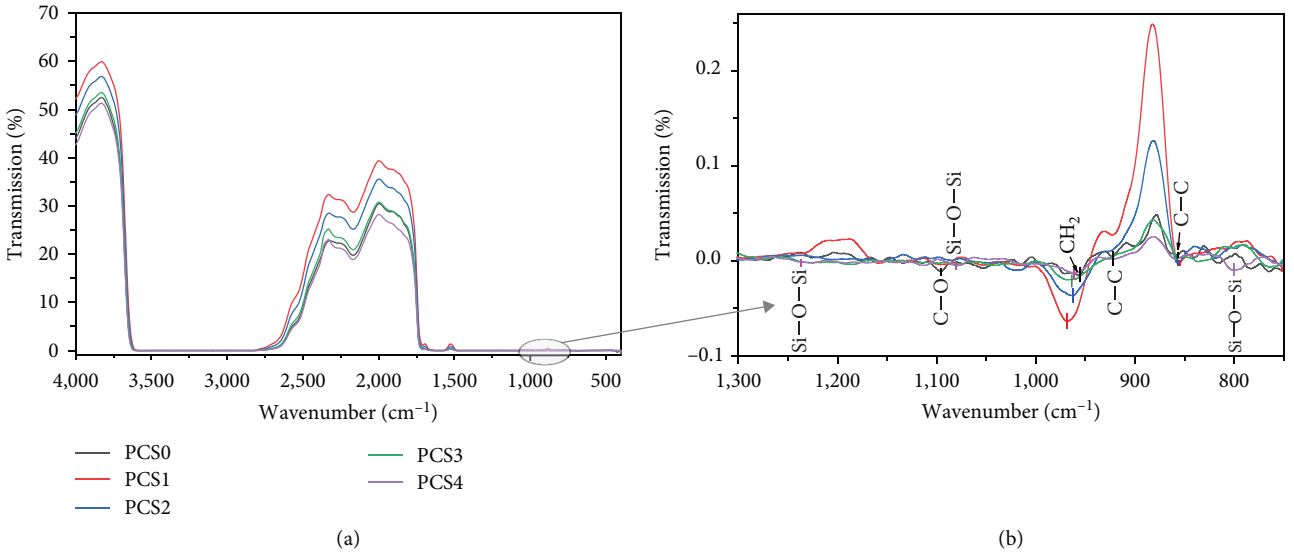

Figure 1: (a, b) FTIR spectra for PVA/CMC/SiO_2 films.

Table 1: FTIR bands assignment of PVA/CMC blend film.

Wavenumber (cm^{-1})	Assignment
3,287	—OH stretching [32]
2,924	—CH_2 asymmetric stretching [32]
1,720	C═O stretching [32]
1,662	C═C stretching [32]
1,560	C—H and C—O stretching [32, 33]
1,484	CH_2 bending [34]
1,250	—CH_2 bending [35]
1,234	Si—O—Si stretching [36]
1,095	C—O stretching of CMC [35]
920	C—C stretching [37]
957	Rocking vibration of CH_2 [38]
856	C—C stretching [35, 39]
800	Si—O—Si stretching [36]

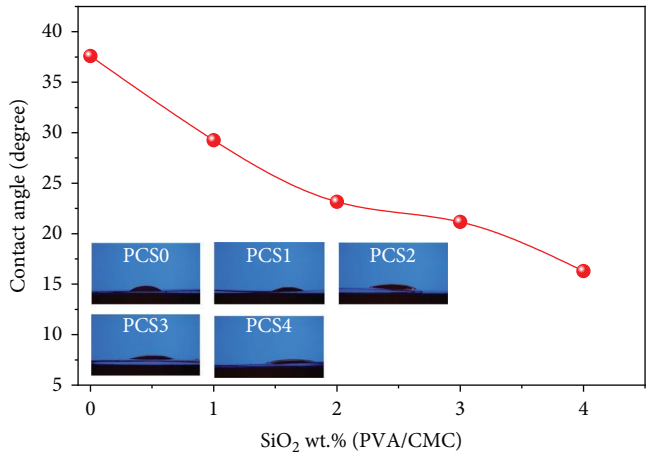

Figure 2: The correlation between the concentration of SiO_2 and the contact angle in the PVA/CMC films.

angle measurement, which indicates the wetting property's degree, can be used to explain the wetting characteristic. Surface wettability of hydrophobic material decreases with increasing contact angle, while surface wettability of hydrophilic material increases with decreasing contact angle [43]. The contact angle value of drop-distilled water on the film surface was measured for PVA/CMC blend film and PVA/CMC films doped with SiO_2. Figure 2 shows the average contact angle (θ), measured on both sides (left and right), of water droplets on the surface of the PCS blend films. The angle of contact decreases from 37.6° for PCS0 to about 29.3°, 23.2°, 21.2°, and 16.3° for PCS1, PCS2, PCS3, and PCS4, respectively, as the SiO_2 concentration increases in the blend film. This affirms the more hydrophilicity of the blend film after the inclusion of SiO_2, owing to SiO_2's high hydrophilicity [26]. The reduction in contact angle is an indication of the increase in wettability with increasing SiO_2 concentrations. Consequently, micropores could be formed because of enhancement of the wettability and it may cause a change in the surface roughness. The surface roughness for PVA/CMC blend films with the effect of various concentrations of SiO_2 was investigated, as shown in Figure 3. From the roughness curves, the roughness parameters were extracted, and Table 2 presents the results. It is crucial to note that R_a signifies the mean height, R_p is the maximum peak height, R_q is the root mean square profile height, R_v is the maximum valley depth, and R_z is the average maximum height [44, 45].

It is obvious that the values of R_a, R_z, R_p, R_q, and R_v all increase with increasing SiO_2 concentration in the blend film. It confirms the rise in film roughness with increasing SiO_2 concentrations. This impact of SiO_2 nanoparticles on the surface roughness is consistent with previous observations for PVDF-HFP [30, 46]. PVA and CMC are hydrophilic polymers, in contrast to PVDF, which is a hydrophobic polymer. The contact angle of the PVDF film was found to increase with increasing SiO_2 concentrations, while here the contact

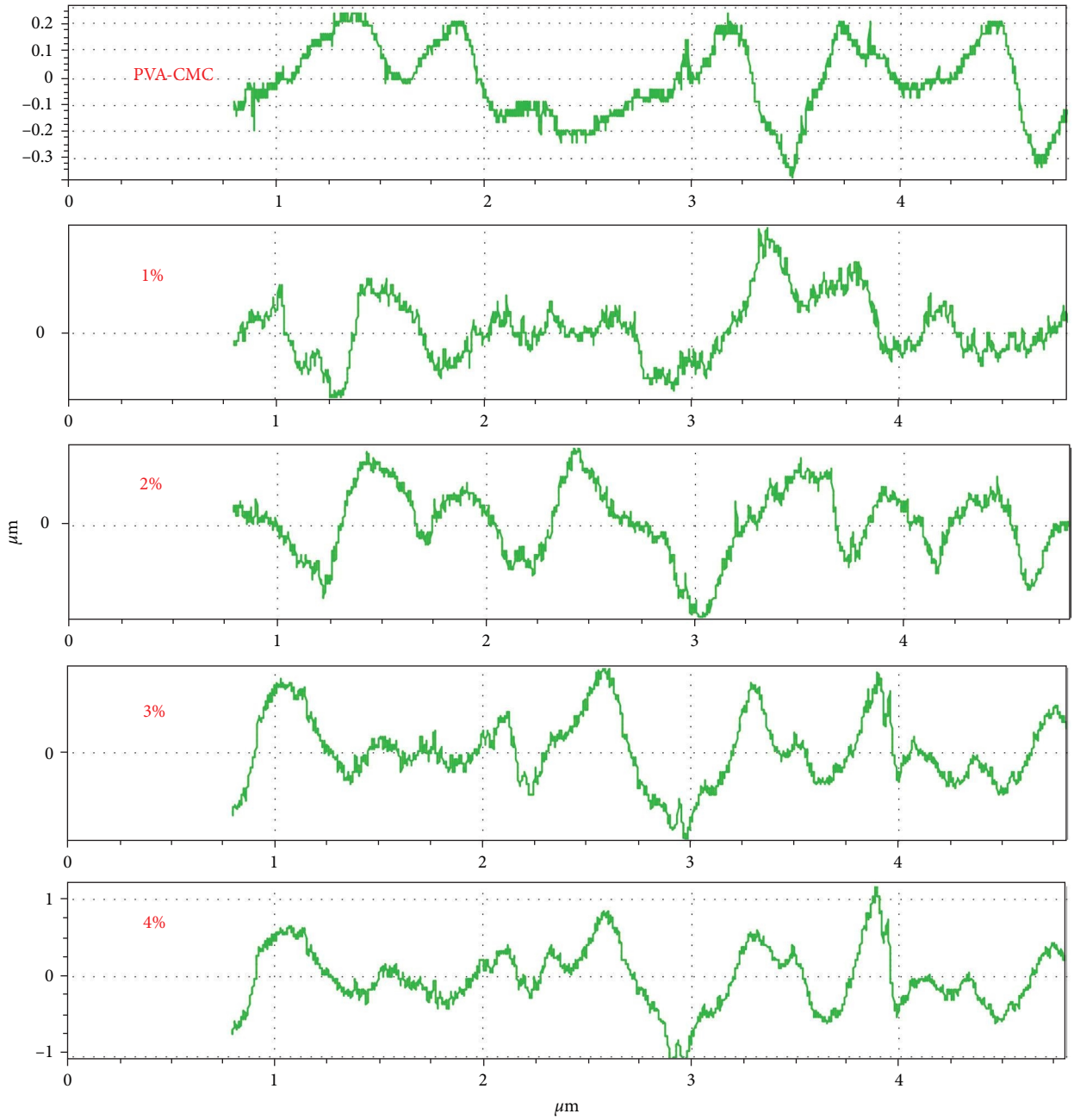

Figure 3: Roughness curves for PVA/CMC/SiO_2 blend films.

Table 2: Roughness parameters of PVA/CMC/SiO_2 films.

Sample ID	R_a	R_z	R_q	R_p	R_v	R_{sk}	R_{ku}	R_k
PCS0	0.123	0.521	0.146	0.241	0.28	−0.209	2.032	0.406
PCS1	0.186	0.739	0.218	0.381	0.357	−0.287	2.079	0.553
PCS2	0.232	1.028	0.276	0.526	0.502	0.115	2.017	0.665
PCS3	0.296	1.274	0.354	0.705	0.57	0.41	2.212	0.86
PCS4	0.322	1.424	0.382	0.758	0.666	0.209	2.139	1.023

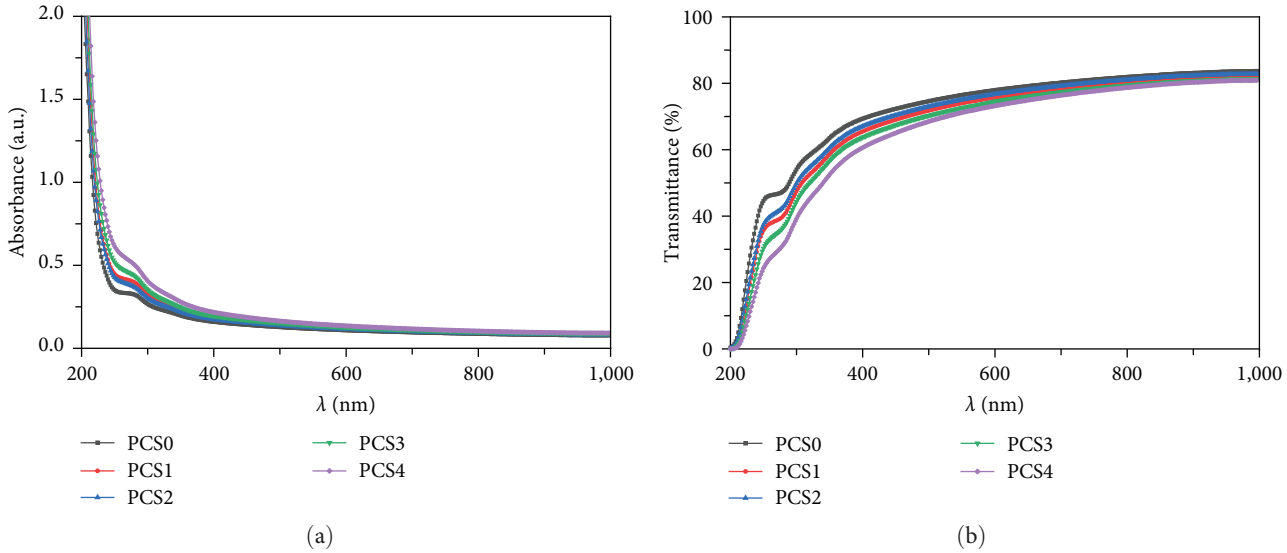

FIGURE 4: Plot of (a) absorbance and (b) transmittance vs. (λ) for PVA/CMC/SiO_2 films.

angle was found to decrease with increasing SiO_2 concentrations. The skewness parameter (R_{sk}) indicates the degree of surface unevenness of a polymer film. A negative value of R_{sk} indicates a flat surface, while a positive value indicates the presence of peaks and deep scratches. As shown in Table 2, the R_{sk} values for PCS0 and PCS1 samples are negative, revealing low roughness of the film surface [44]. The R_{sk} values for the others, PCS2, PCS3, and PCS4, are positive and show an increase with increasing SiO_2 concentrations, which reveals the increase in the roughness of the film's surface.

3.2. Optical Properties. The spectra (transmittance and absorption) of PVA/CMC films as a function of the incident light wavelength (λ) are displayed in Figure 4. Obviously, the absorbance of the blend films increases gradually with increasing the SiO_2 concentrations, as shown in Figure 4(a). In addition to the shift in the absorption edge toward the higher wavelength region, indicating to the decrease in the bandgap of the blend films. The hump observed at about 276 nm is related to the π–π^* transition [45].

With a rise in SiO_2 concentrations, the transmittance of blended films goes down, as shown in Figure 4(b). This highlights the importance of controlling the concentration of SiO_2 to ensure maximum transmittance and, ultimately, optimal performance of the blended films. In the visible-region around 500 nm, the transparency of the blend films decreases from 75% for PCS0 to about 73%, 72%, 70%, and 68% for PCS1, PCS2, PCS3, and PCS4, respectively. The addition of SiO_2 to the blend matrix causes an increase in the number of absorbed atoms and, of course, a decrease in the transmittance of light. The observed influence of SiO_2 on optical transmittance aligns with previous findings documented in the literature [31]. The film absorption coefficient (α) is determined using the absorbance (A) and the film thickness (t) according to the following relation [47]:

$$\alpha = \frac{2.303 \times A}{t}. \tag{1}$$

According to this, the optical parameters, which include E_{gd} (direct-bandgap), E_{gi} (indirect-bandgap), E_U (tail–band–width, or Urbach energy), n (refractive-index), k (extinction coefficient), ε' (optical dielectric constant), ε'' (optical dielectric loss), and $\sigma_{opt.}$ (optical conductivity), can be calculated using the following relations [33]:

$$(\alpha h\upsilon)^2 = B_1\left(h\upsilon - E_{gd}\right), \tag{2}$$

$$(\alpha h\upsilon)^{1/2} = B_2\left(h\upsilon - E_{gi}\right), \tag{3}$$

$$\mathrm{Ln}\,\alpha = \ln\alpha_0 + \frac{h\upsilon}{E_U}, \tag{4}$$

$$n = \left(\frac{1+R}{1-R}\right) + \sqrt{\frac{4R}{(1-R)^2} - k^2}, \tag{5}$$

$$k = \frac{\alpha\lambda}{4\pi}, \tag{6}$$

$$\varepsilon_r = n^2 - k^2, \tag{7}$$

$$\varepsilon_i = 2\mathrm{nk}, \tag{8}$$

$$\sigma_{opt.} = \frac{\alpha n C}{4\pi}, \tag{9}$$

where B_1 and B_2 are constants, and C is the speed of light (3×10^8 m/s).

As illustrated in Figure 5, the E_{gd} and E_{gi} are derived from the relation between $(\alpha h\upsilon)^2$ and $(\alpha h\upsilon)^{1/2}$ versus $(h\upsilon)$,

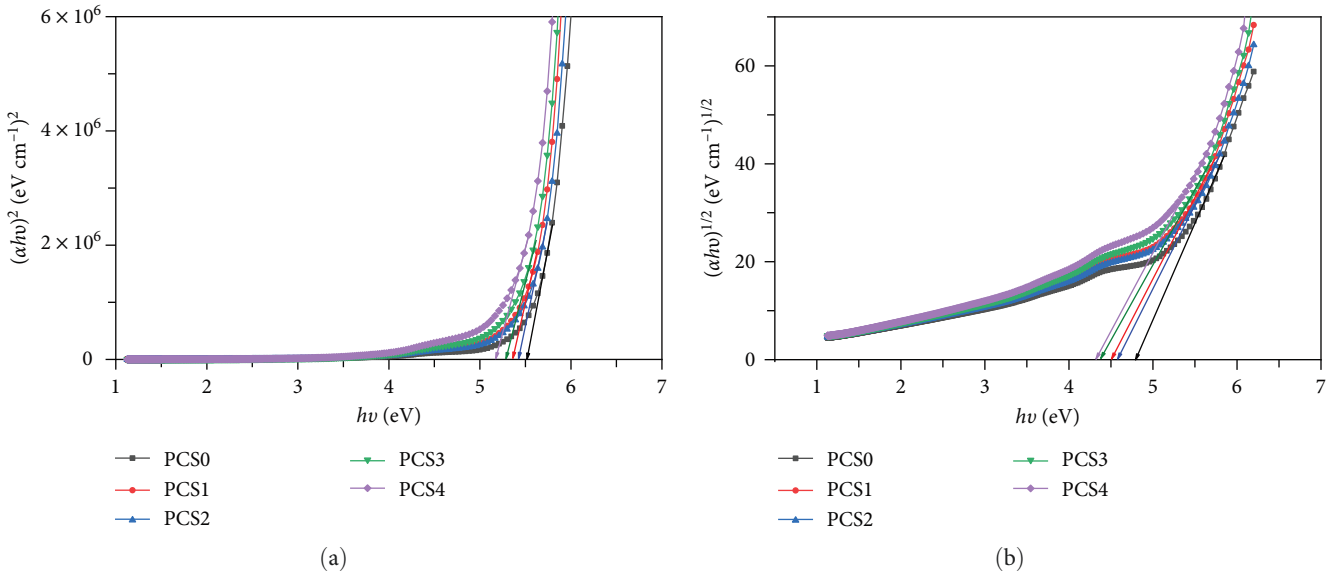

FIGURE 5: The dependences of $(\alpha h\upsilon)^2$ (a) and $(\alpha h\upsilon)^{1/2}$ (b) on $(h\upsilon)$ for PVA/CMC/SiO_2 films.

TABLE 3: Optical parameters for PVA/CMC/SiO_2 films.

Film ID	E_{gd} (eV)	E_{gi} (eV)	E_U (eV)	n ($\lambda = 600$ nm)
PCS0	5.52	4.79	0.84	2.009
PCS1	5.36	4.51	0.83	2.074
PCS2	5.42	4.57	0.86	2.047
PCS3	5.28	4.38	0.87	2.106
PCS4	5.17	4.32	0.91	2.144

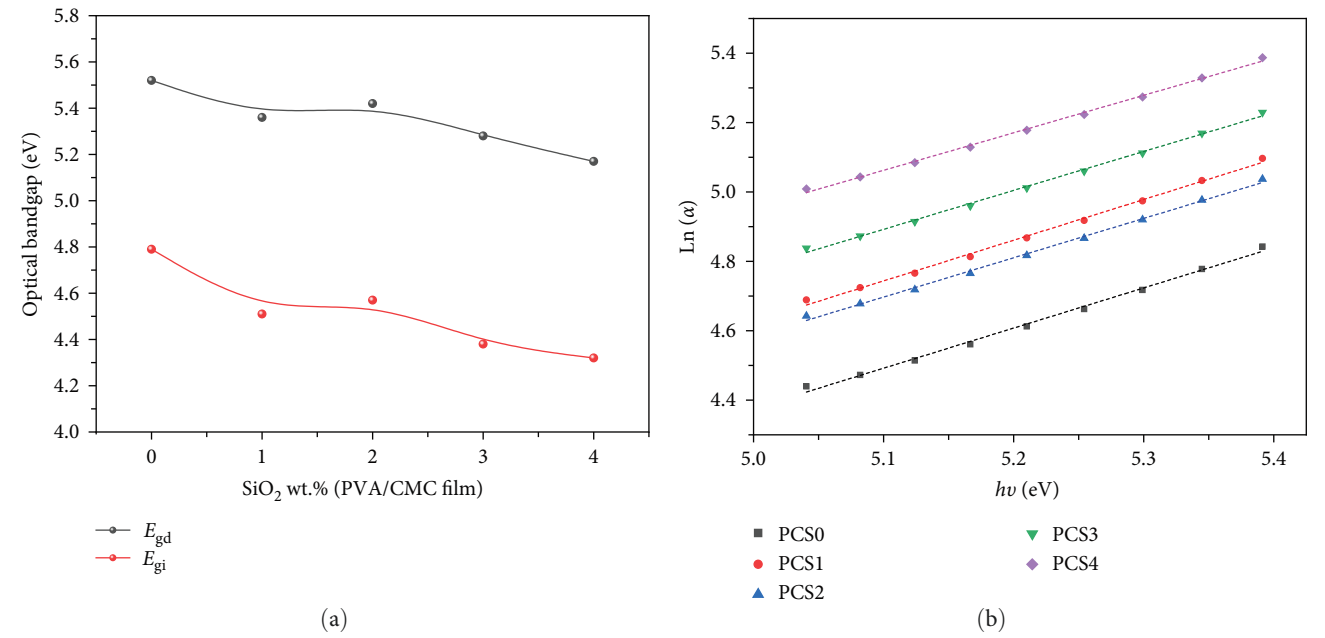

FIGURE 6: (a) Optical bandgap dependence on SiO_2 content in PVA/CMC film, and (b) ln (α) vs. $h\upsilon$ for PVA/CMC/SiO_2 films.

respectively. The E_{gd} for the pure PVA/CMC blend film is about 5.52 eV, which is consistent with previous work [18, 19]. From Table 3, the E_{gd} and E_{gi} values slightly decreased with increasing the SiO_2 concentrations in the PVA/CMC blend film. Figure 6(a) displays the variation of the optical bandgap (E_{gd} and E_{gi}) values with the SiO_2 content in the PVA/CMC blend film. It shows a decline in the bandgap value as the SiO_2 content increases in the blend

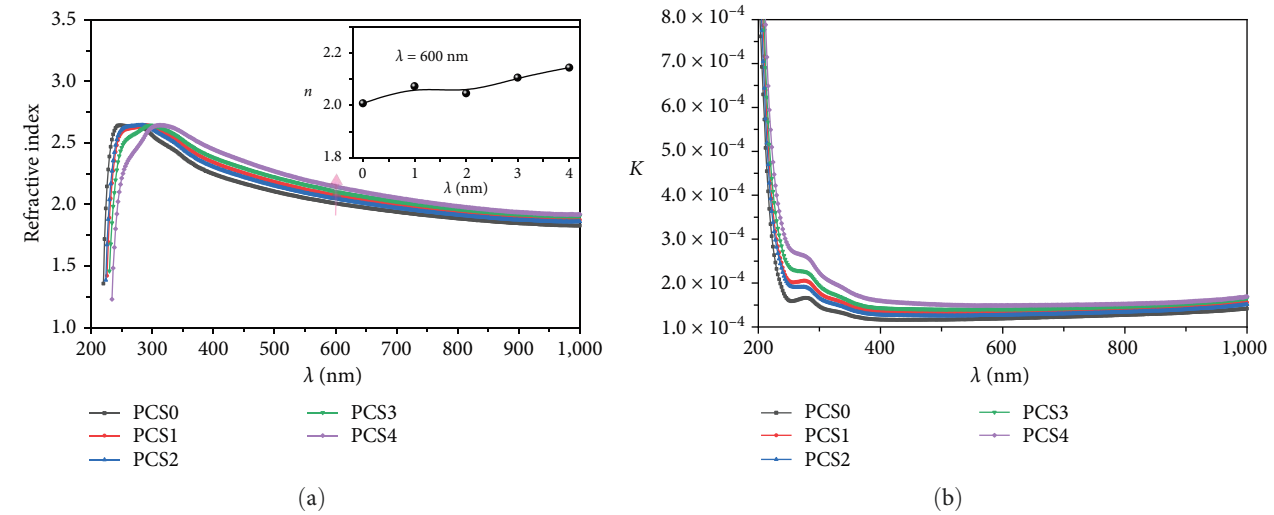

FIGURE 7: The wavelength-dependent n (a) and k (b) for PVA/CMC/SiO_2 films.

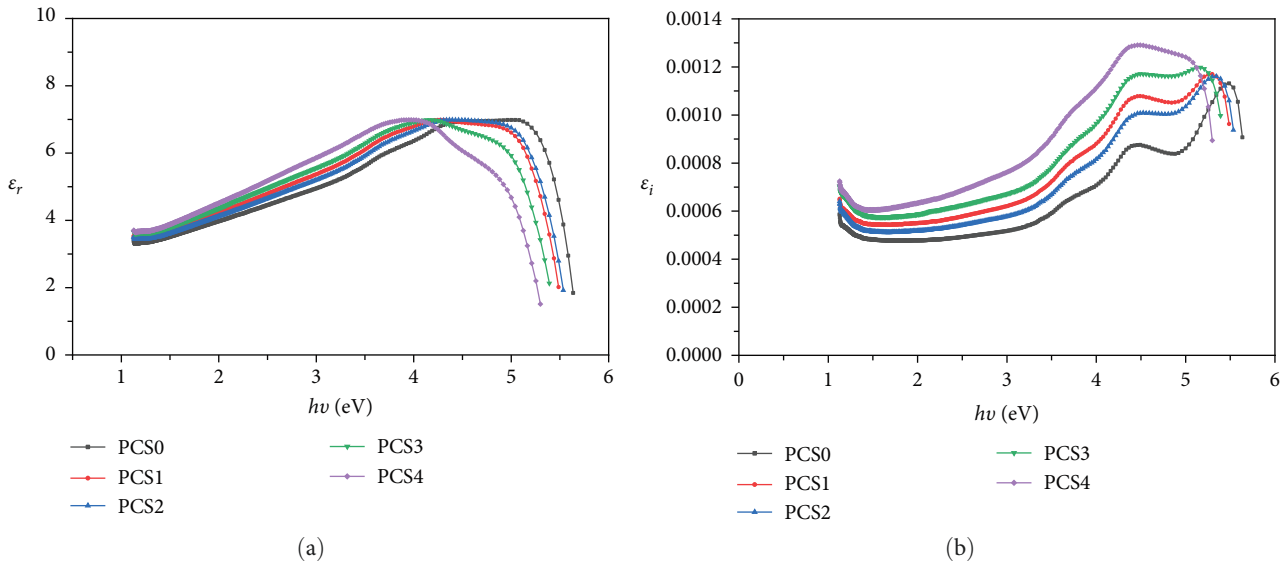

FIGURE 8: The dependences of ε_r (a) and ε_i (b) vs. ($h\upsilon$) for PVA/CMC/SiO_2 films.

matrix. This behavior is related to the defects created as the SiO_2 is added to the blend matrix, and this result is in good accordance with the literature [20, 48]. The phenomenon could be associated with the interactions between the molecules of the blend matrix and the SiO_2 atoms. These interactions may form a hydrogen bond that creates localized states within the forbidden energy zone and reduces the distance between the valence and conduction bands. This disorder and defects created were affirmed by investigation of the tail width, Urbach energy (E_U), of the blend films using Equation (4) [49]. The linear portion from the relation between ln (α) and ($h\upsilon$), Figure 6(b), is the reciprocal of E_U. It is clear from Table 3 that the E_U value increases from 0.84 eV for PCS0 to about 0.91 eV for PCS4, confirming the blend matrix's increasing disordering and bandgap decreasing.

According to Equations (5) and (6), n and k values are computed regarding λ, as shown in Figure 7. Evidently, n and k both rose as SiO_2 concentrations increased and fell as incident light wavelengths increased.

As the SiO_2 concentration increases in the blend matrix, the number of atoms colliding with incident light increases and the reflectivity of the films increases as well. As a result, the refractive index rises along with the slowing of light velocity inside the blend matrix. On the other hand, the k value represents the loss of energy caused by light scattered or absorbed by the material [50]. As shown in Figure 7(b), it showed a normal behavior in the UV region, as it decreases sharply as it is related to the bandgap region, which has high energy sufficient to be absorbed and the loss caused by scattered or absorbed light will be less.

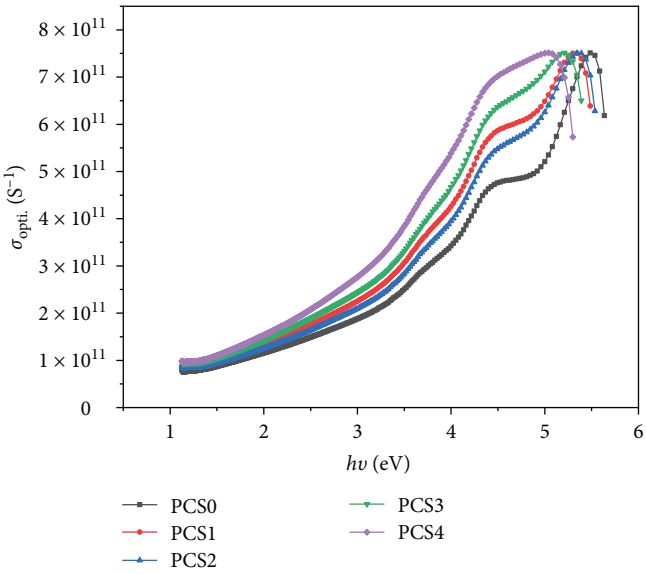

FIGURE 9: The $\sigma_{opt.}$ vs. ($h\upsilon$) for PVA/CMC/SiO_2 films.

The ε_r and ε_i as a function of the $h\upsilon$ are illustrated in Figure 8. Both optical parameters are increased with increasing the SiO_2 concentrations in the PVA/CMC blend films. An increase in ε_r value is directly proportional to the higher density of states within the bandgap, resulting from the increased concentration of SiO_2 [51, 52]. In addition, the ε_i value increased with increasing SiO_2 concentration, and the absorption band at the higher photon energy region shifted toward the lower photon energy. This is explained by the fact that as SiO_2 concentration rises, the number of free charge carriers in the matrix also rises [51].

The optical conductivity ($\sigma_{opt.}$) dependence on photon energy is displayed in Figure 9. It shows an increase in $\sigma_{opt.}$ with increasing SiO_2 concentrations, which could be due to the rise in charge carriers in the blend films.

The SiO_2 impact on the $\sigma_{opt.}$ of PVA/CMC films results from the transfer of charge between the blend's molecules and SiO_2 [53]. The interstitial spaces between the matrix chains are filled by SiO_2 and form a segregated network [54]. Hence, the optical conductivity increases as well.

4. Conclusion

Probe sonication and casting solution techniques were utilized for preparing the blend matrix of PVA/CMC with various amounts of SiO_2. The FTIR analysis revealed the interaction between the blend matrix molecules and SiO_2 nanoparticles. The contact angle and surface roughness parameter investigations confirm the modification of the PVA/CMC surface after the inclusion of SiO_2, where the surface roughness and surface wettability of the PVA/CMC matrix were increased. This is related to the hydrophilic of the SiO_2 nanoparticles. The optical analysis showed a slight decrease in the blend film transparency with increasing the SiO_2 amount, and a redshift was observed in the absorption edge, which confirms the reduction of the optical bandgap energy. The decrease in transparency and increase in film absorption raise their possibility of being used in UV-shielding applications. Th optical bandgap decreases from 5.52 eV for pure PVA/CMC to 5.17 eV for the PVA/CMC/4 wt.% SiO_2. This drop was related to the defects in the materials, and the refractive index rises due to increasing matrix density. The prepared current matrix, PVA/CMC/SiO_2, is considered a potential candidate for optical applications.

Data Availability

All the data are available in the manuscript.

Conflicts of Interest

The author declares that there are no conflicts of interest.

References

[1] E. M. M. Abdelrazek, A. M. Abdelghany, S. I. Badr, and M. A. Morsi, "Structural, optical, morphological and thermal properties of PEO/PVP blend containing different concentrations of biosynthesized Au nanoparticles," *Journal of Materials Research and Technology*, vol. 7, no. 4, pp. 419–431, 2018.

[2] S. S. Pesetskii, O. V. Filimonov, V. N. Koval, and V. V. Golubovich, "Structural features and relaxation properties of PET/PC blends containing impact strength modifier and chain extender," *Express Polymer Letters*, vol. 3, no. 10, pp. 606–614, 2009.

[3] G. Nuroldayeva and M. P. Balanay, "Flexing the spectrum: advancements and prospects of flexible electrochromic materials," *Polymers*, vol. 15, no. 13, Article ID 2924, 2023.

[4] H. M. Alghamdi and A. Rajeh, "Synthesis of $CoFe_2O_4$/MWCNTs nanohybrid and its effect on the optical, thermal, and conductivity of PVA/CMC composite as an application in electrochemical devices," *Journal of Inorganic and Organometallic Polymers and Materials*, vol. 32, no. 5, pp. 1935–1949, 2022.

[5] A. M. Meftah, E. Gharibshahi, N. Soltani, W. M. M. Yunus, and E. Saion, "Structural, optical and electrical properties of PVA/PANI/Nickel nanocomposites synthesized by gamma radiolytic method," *Polymers*, vol. 6, no. 9, pp. 2435–2450, 2014.

[6] J. Zhu, Q. Li, Y. Che et al., "Effect of Na_2CO_3 on the microstructure and macroscopic properties and mechanism analysis of PVA/CMC composite film," *Polymers*, vol. 12, no. 2, Article ID 453, 2020.

[7] M. B. Mohamed and M. H. Abdel-Kader, "Effect of excess oxygen content within different nano-oxide additives on the structural and optical properties of PVA/PEG blend," *Applied Physics A*, vol. 125, no. 3, Article ID 209, 2019.

[8] M. F. Zaki, S. I. Elkalashy, S. A. Vshivkov, and T. S. Soliman, "Synthesis, structural, and physical properties of polyvinyl alcohol/carboxymethyl cellulose blend films induced by gamma-irradiation," *Optical and Quantum Electronics*, vol. 55, no. 11, 2023.

[9] Z. Yang, H. Peng, W. Wang, and T. Liu, "Crystallization behavior of poly(ε-caprolactone)/layered double hydroxide nanocomposites," *Journal of Applied Polymer Science*, vol. 116, no. 5, pp. 2658–2667, 2010.

[10] M. M. Abutalib and A. Rajeh, "Boosting optical and electrical characteristics of polyvinyl alcohol/carboxymethyl cellulose nanocomposites by GNPs/MWCNTs fillers as an application

in energy storage devices," *International Journal of Energy Research*, vol. 46, no. 5, pp. 6216–6224, 2022.

[11] N. M. Shaalan, T. A. Hanafy, and M. Rashad, "Dual optical properties of NiO-doped PVA nanocomposite films," *Optical Materials*, vol. 119, Article ID 111325, 2021.

[12] M. A. Hoque, M. R. Ahmed, G. T. Rahman et al., "Fabrication and comparative study of magnetic Fe and α-Fe_2O_3 nanoparticles dispersed hybrid polymer (PVA + Chitosan) novel nanocomposite film," *Results in Physics*, vol. 10, pp. 434–443, 2018.

[13] J. Selvi, V. Parthasarathy, S. Mahalakshmi, R. Anbarasan, M. O. Daramola, and P. S. Kumar, "Optical, electrical, mechanical, and thermal properties and non-isothermal decomposition behavior of poly(vinyl alcohol)–ZnO nanocomposites," *Iranian Polymer Journal*, vol. 29, no. 5, pp. 411–422, 2020.

[14] S. Alhassan, M. Alshammari, K. Alshammari et al., "Preparation and optical properties of PVDF-$CaFe_2O_4$ polymer nanocomposite films," *Polymers*, vol. 15, no. 9, Article ID 2232, 2023.

[15] S. Ningaraju, A. P. G. Prakash, and H. B. Ravikumar, "Studies on free volume controlled electrical properties of PVA/NiO and PVA/TiO_2 polymer nanocomposites," *Solid State Ionics*, vol. 320, pp. 132–147, 2018.

[16] F. Ahmad and M. A. Hassan, "Structure and physical properties of Al_2O_3 nanofillers embedded in poly(vinyl alcohol)," *Polymer Composites*, vol. 40, no. S1, pp. E647–E653, 2019.

[17] T. A. Taha, N. Hendawy, S. El-Rabaie, A. Esmat, and M. K. El-Mansy, "Effect of NiO NPs doping on the structure and optical properties of PVC polymer films," *Polymer Bulletin*, vol. 76, no. 9, pp. 4769–4784, 2019.

[18] T. S. Soliman, H. M. Abomostafa, and A. S. Abouhaswa, "Synthesis of Ni0.8Mg0.2Fe_2O_4 nanoparticles and its impact in enhancing the structural, magnetic, and optical properties of the PVA-CMC polymer blend," *Inorganic Chemistry Communications*, vol. 164, Article ID 112408, 2024.

[19] A. S. Abouhaswa, G. M. Turky, and T. S. Soliman, "Structural, optical, and dielectric properties of PVA-CMC/Ni0.65Cu0.35-Fe_2O_4 films for optoelectronic applications and energy storage applications," *Journal of Inorganic and Organometallic Polymers and Materials*, vol. 34, no. 4, pp. 1699–1711, 2024.

[20] A. Badawi, "Engineering the optical properties of PVA/PVP polymeric blend in situ using tin sulfide for optoelectronics," *Applied Physics A*, vol. 126, no. 5, Article ID 335, 2020.

[21] A. Badawi, S. S. Alharthi, A. A. Alotaibi, and M. G. Althobaiti, "Investigation of the mechanical and electrical properties of SnS filled PVP/PVA polymeric composite blends," *Journal of Polymer Research*, vol. 28, no. 6, 2021.

[22] S. S. Alharthi, M. G. Althobaiti, A. A. Alkathiri, E. E. Ali, and A. Badawi, "Exploring the functional properties of PVP/PVA blend incorporated with non-stoichiometric SnS for optoelectronic devices," *Journal of Taibah University for Science*, vol. 16, no. 1, pp. 317–329, 2022.

[23] S. S. Alharthi and A. Badawi, "Tailoring the linear and nonlinear optical characteristics of PVA/PVP polymeric blend using Co0.9Cu0.1S nanoparticles for optical and photonic applications," *Optical Materials*, vol. 127, Article ID 112255, 2022.

[24] S. S. Alharthi and A. Badawi, "Effect of Ag/CuS nanoparticles loading to enhance linear/nonlinear spectroscopic and electrical characteristics of PVP/PVA blends for flexible optoelectronics," *Journal of Vinyl and Additive Technology*, vol. 30, no. 1, pp. 230–243, 2024.

[25] S. Choudhary, "Characterization of amorphous silica nanofiller effect on the structural, morphological, optical, thermal, dielectric and electrical properties of PVA–PVP blend based polymer nanocomposites for their flexible nanodielectric applications," *Journal of Materials Science: Materials in Electronics*, vol. 29, no. 12, pp. 10517–10534, 2018.

[26] K. Deshmukh, M. B. Ahamed, K. K. Sadasivuni et al., "Fumed SiO_2 nanoparticle reinforced biopolymer blend nanocomposites with high dielectric constant and low dielectric loss for flexible organic electronics," *Journal of Applied Polymer Science*, vol. 134, no. 5, Article ID 44427, 2017.

[27] R. S. A. Hamza and M. A. Habeeb, "Reinforcement of morphological, structural, optical, and antibacterial characteristics of PVA/CMC bioblend filled with SiO_2/Cr_2O_3 hybrid nanoparticles for optical nanodevices and food packing industries," *Polymer Bulletin*, vol. 81, no. 5, pp. 4427–4448, 2024.

[28] R. S. A. Hamza and M. A. Habeeb, "Fabrication and exploring the morphological, structural and optical characteristics of polyvinyl alchol—carboxymethyl cellulose—silicon dioxide—tin dioxide nanostructures for optoelectronics and antibacterial applications," *Silicon*, vol. 16, no. 3, pp. 1043–1056, 2024.

[29] G. Wu, Y. Yang, Y. Lei et al., "Hydrophilic nano-SiO_2/PVA-based coating with durable antifogging properties," *Journal of Coatings Technology and Research*, vol. 17, no. 5, pp. 1145–1155, 2020.

[30] M. J. Toh, P. C. Oh, T. L. Chew, and A. L. Ahmad, "Antiwettability enhancement of PVDF-HFP membrane via superhydrophobic modification by SiO_2 nanoparticles," *Comptes Rendus. Chimie*, vol. 22, no. 5, pp. 369–372, 2019.

[31] E. M. Baba, C. E. Cansoy, and E. O. Zayim, "Investigation of wettability and optical properties of superhydrophobic polystyrene-SiO_2 composite surfaces," *Progress in Organic Coatings*, vol. 99, pp. 378–385, 2016.

[32] R. M. Ahmed, T. S. Soliman, S. A. Vshivkov, and A. Khalid, "Influence of Fe_2O_3 @reduced graphene oxide nanocomposite on the structural, morphological, and optical features of the polyvinyl alcohol films for optoelectronic applications," *Physica Scripta*, vol. 98, no. 5, Article ID 055928, 2023.

[33] T. S. Soliman, M. M. Hessien, and S. I. Elkalashy, "Structural, thermal, and optical properties of polyvinyl alcohol films doped with La_2ZnOx nanoparticles," *Journal of Non-Crystalline Solids*, vol. 580, Article ID 121405, 2022.

[34] M. S. Toman and S. H. Al-Nesrawy, "New fabrication (PVA-CMC -PbO) nanocomposites structural and electrical properties," *NeuroQuantology*, vol. 19, pp. 38–46, 2021.

[35] A. A. Al-Muntaser, R. A. Pashameah, K. Sharma, E. Alzahrani, M. O. Farea, and M. A. Morsi, "α-MoO_3 nanobelts/CMC-PVA nanocomposites: hybrid materials for optoelectronic and dielectric applications," *Journal of Polymer Research*, vol. 29, pp. 1–11, 2022.

[36] C.-C. Yang, Y. J. Li, and T.-H. Liou, "Preparation of novel poly (vinyl alcohol)/SiO_2 nanocomposite membranes by a sol–gel process and their application on alkaline DMFCs," *Desalination*, vol. 276, no. 1–3, pp. 366–372, 2011.

[37] H. E. Ali, M. M. Abdel-Aziz, Y. Khairy et al., "Microstructure analysis and nonlin-ear/linear optical parameters of polymeric composite fil-ms based PVAL for wi-de optical applications," *Physica Scripta*, vol. 96, no. 11, Article ID 115804, 2021.

[38] Z. K. Heiba, M. B. Mohamed, A. Badawi, and A. A. Alhazime, "The role of Cd0.9Mg0.1S nanofillers on the structural, optical, and dielectric properties of PVA/CMC polymeric blend," *Chemical Physics Letters*, vol. 770, Article ID 138460, 2021.

[39] M. R. Atta, Q. A. Alsulami, G. M. Asnag, and A. Rajeh, "Enhanced optical, morphological, dielectric, and conductivity properties of gold nanoparticles doped with PVA/CMC blend as an application in organoelectronic devices," *Journal of Materials Science: Materials in Electronics*, vol. 32, no. 8, pp. 10443–10457, 2021.

[40] B. Karthikeyan, S. Hariharan, A. Sasidharan et al., "Optical, vibrational and fluorescence recombination pathway properties of nano SiO_2-PVA composite films," *Optical Materials*, vol. 90, pp. 139–144, 2019.

[41] S. Radoor, J. Karayil, J. Parameswaranpillai, and S. Siengchin, "Adsorption of methylene blue dye from aqueous solution by a novel PVA/CMC/halloysite nanoclay bio composite: characterization, kinetics, isotherm and antibacterial properties," *Journal of Environmental Health Science and Engineering*, vol. 18, no. 2, pp. 1311–1327, 2020.

[42] H. A. Budiarti, R. N. Puspitasari, A. M. Hatta, Sekartedjo, and D. D. Risanti, "Synthesis and Characterization of TiO_2 @SiO_2 and SiO_2 @TiO_2 core-shell structure using lapindo mud extract via sol-gel method," *Procedia Engineering*, vol. 170, pp. 65–71, 2017.

[43] M. F. Zaki, A. M. A. Reheem, H. H. Mahmoud, and S. I. Elkalashy, "Amendment the surface structure and optical properties of Makrofol LT by low energy oxygen ion bombardment," *Applied Radiation and Isotopes*, vol. 192, Article ID 110594, 2023.

[44] T. S. Soliman, "Effect of CdSSe nanoparticles on the structural, surface roughness, linear, and nonlinear optical parameters of polyvinyl chloride films for optoelectronic applications," *Physica Scripta*, vol. 98, no. 7, Article ID 075932, 2023.

[45] T. S. Soliman, S. A. Vshivkov, M. M. Hessien, and S. I. Elkalashy, "Impact of Mn–Ni spinal ferrite nanoparticles on and optical parameters of polyvinyl alcohol for," *Soft Matter*, vol. 19, no. 40, pp. 7753–7763, 2023.

[46] A. Ghaee, A. Ghadimi, B. Sadatnia, A. F. Ismail, Z. Mansourpour, and M. Khosravi, "Synthesis and characterization of poly(vinylidene fluoride) membrane containing hydrophobic silica nanoparticles for CO_2 absorption from CO_2/N_2 using membrane contactor," *Chemical Engineering Research and Design*, vol. 120, pp. 47–57, 2017.

[47] A. M. Salem, A. R. Mohamed, A. M. Abdelghany, and A. Y. Yassin, "Effect of polypyrrole on structural, optical and thermal properties of CMC-based blends for optoelectronic applications," *Optical Materials*, vol. 134, Article ID 113128, 2022.

[48] A. Badawi, S. S. Alharthi, H. Assaedi, A. N. Alharbi, and M. G. Althobaiti, "Cd0.9Co0.1S nanostructures concentration study on the structural and optical properties of SWCNTs/PVA blend," *Chemical Physics Letters*, vol. 775, Article ID 138701, 2021.

[49] M. F. Zaki, S. I. Elkalashy, and T. S. Soliman, "A comparative study of the structural, optical and morphological properties of different types of Makrofol polycarbonate," *Polymer Bulletin*, vol. 79, no. 12, pp. 10841–10863, 2022.

[50] T. S. Soliman, S. A. Vshivkov, A. I. Abdel-Salam, I. Gomaa, and A. Khalid, "Structural and optical parameters of polyvinyl alcohol films reinforced with Mn_2O_3/reduced graphene oxide composite," *Physica Scripta*, vol. 98, no. 1, Article ID 15832, 2022.

[51] S. B. Aziz, "Modifying poly(vinyl alcohol) (PVA) from Insulator to small-bandgap polymer: a novel approach for organic solar cells and optoelectronic devices," *Journal of Electronic Materials*, vol. 45, no. 1, pp. 736–745, 2016.

[52] R. Abdullah, S. Aziz, S. Mamand, A. Hassan, S. Hussein, and M. Kadir, "Reducing the crystallite size of spherulites in PEO-based polymer nanocomposites mediated by carbon nanodots and Ag nanoparticles," *Nanomaterials*, vol. 9, no. 6, Article ID 874, 2019.

[53] T. S. Soliman and A. S. Abouhaswa, "Synthesis and structural of $Cd0.5Zn0.5F_2O_4$ nanoparticles and its influence on the structure and optical properties of polyvinyl alcohol films," *Journal of Materials Science: Materials in Electronics*, vol. 31, no. 12, pp. 9666–9674, 2020.

[54] O. G. Abdullah, S. B. Aziz, K. M. Omer, and Y. M. Salih, "Reducing the optical band gap of polyvinyl alcohol (PVA) based nanocomposite," *Journal of Materials Science: Materials in Electronics*, vol. 26, no. 7, pp. 5303–5309, 2015.